SEDIMENTOLOGY the journal of the International Association of Sedimentologists

Sedimentology (2019) doi: 10.1111/sed.12591

Constraining sediment provenance for tsunami deposits using distributions of grain size and foraminifera from the Kujukuri coastline and shelf, Japan

JESSICA E. PILARCZYK*†‡, YUKI SAWAI‡, DAN MATSUMOTO‡, YUICHI NAMEGAYA‡, NAOHISA NISHIDA‡[1], KEN IKEHARA‡, OSAMU FUJIWARA‡, CHRIS GOURAMANIS§, TINA DURA¶ and BENJAMIN P. HORTON**††

**Centre for Natural Hazards Research, Department of Earth Sciences, Simon Fraser University, Burnaby, BC, V5A 1S6, Canada (E-mail: jessica_pilarczyk@sfu.ca)*

†School of Ocean Science and Technology, Division of Marine Science, University of Southern Mississippi, Stennis Space Center, MS, 39529, USA

‡Geological Survey of Japan, National Institute of Advanced Industrial Science and Technology (AIST), Tsukuba, Japan

§Department of Geography, Faculty of Arts and Social Sciences, National University of Singapore, Singapore, Singapore

¶Department of Geology, Humboldt State University, Arcata, CA, 95521, USA

***Asian School of the Environment, Nanyang Technological University, Singapore, Singapore*

††Earth Observatory of Singapore, Nanyang Technological University, Singapore, Singapore

Associate Editor – Pedro Costa

ABSTRACT

Tsunami deposits preserved in the geological record provide a more comprehensive understanding of their patterns of frequency and intensity over longer timescales; but recognizing tsunami deposits can prove challenging due to post-depositional changes, lack of contrast between the deposits and surrounding sedimentary layers, and differentiating between tsunami and storm deposition. Modern baseline studies address these challenges by providing insight into modern spatial distributions that can be compared with palaeotsunami deposits. This study documents the spatial fingerprint of grain size and foraminifera from Hasunuma Beach and the Kujukuri shelf to provide a basis from which tsunami deposits can be interpreted. At Hasunuma Beach, approximately 50 km east of Tokyo, the spatial distribution of three common proxies (foraminiferal taxonomy, foraminiferal taphonomy and sediment grain size) for tsunami identification were mapped and clustered using Partitioning Around Medoids cluster analysis. Partitioning Around Medoids cluster analysis objectively discriminated two coastal zones corresponding to onshore and offshore sample locations. Results show that onshore samples are characterized by coarser grain sizes (medium to coarse sand) and higher abundances of *Pararotalia nipponica* (27 to 63%) than offshore samples, which are characterized by finer grain sizes (fine to medium sand), lower abundances of *Pararotalia nipponica* (2 to 19%) and *Ammonia parkinsoniana* (0 to 10%), higher abundances of planktonics (15 to 58%) and species with fragile tests including *Uvigerinella glabra*. When compared to grain-size and foraminiferal taxonomy, foraminiferal taphonomy; i.e. surface condition of foraminifera, a proxy not commonly used to identify tsunami deposits, was most effective in discriminating modern coastal zones

[1]Present address: Department of Environmental Sciences, Tokyo Gakugei University, Tokyo, 184-8501, Japan

(identified supratidal, intertidal and offshore environments) and determining sediment provenance for tsunami deposits at Kujukuri. This modern baseline study assists the interpretation of tsunami deposits in the geological record because it provides a basis for sediment provenance to be determined.

Keywords Cluster analysis, coastal hazards, particle-size distribution, taphonomy, typhoon.

INTRODUCTION

The coastlines of eastern Japan have a long history of repeated large earthquakes and tsunamis (e.g. Nanayama *et al.*, 2003; Sawai *et al.*, 2012). Geological studies conducted in Hokkaido (Nanayama *et al.*, 2003, 2007; Sawai *et al.*, 2004, 2009b); Tohoku (Sawai *et al.*, 2012; Tanigawa *et al.*, 2014) and Kanto (Fujiwara & Kamataki, 2007; Shishikura, 2014) have revealed evidence of earthquakes and tsunamis that pre-date the historical record, extending the timeframe of known events back in time by up to 4000 years. These studies are used to assess the long-term seismic trends along subduction zones (e.g. Sawai *et al.*, 2012, 2015).

Assessing the provenance of overwash deposits, such as those from Japan, can provide improved hazard assessment by determining the transport distance and depth from which sediments were entrained (e.g. Uchida *et al.*, 2010; Kosciuch *et al.*, 2018). However, assessing the provenance of anomalous sand layers preserved within coastal sediments is complicated by the presence of a mixture of marine, brackish and terrestrial sediments; an artifact of erosion, transport and deposition of tsunami waves as they inundate the coastline (e.g. Dawson *et al.*, 1996; Grand Pre *et al.*, 2012; Pilarczyk *et al.*, 2014). Detailed modern distribution studies of sedimentological proxies help in this regard because they identify specific sediment sources within coastal, nearshore and offshore environments (e.g. Gischler & Möder, 2009; Pilarczyk *et al.*, 2011; Kosciuch *et al.*, 2018).

The 'proxy toolkit' developed for identifying tsunami deposits in the geological record includes marine-indicative proxies, such as: (i) sediment lithology and stratigraphy (e.g. Atwater, 1987; Pinegina *et al.*, 2003; Cisternas *et al.*, 2005); (ii) microfossils (e.g. Hemphill-Haley, 1995; Hawkes *et al.*, 2007; Dura *et al.*, 2016); (iii) grain size (e.g. Donato *et al.*, 2009; Jaffe *et al.*, 2011; Matsumoto *et al.*, 2016); and (iv) geochemistry (e.g. Minoura & Nakaya, 1991; Chagué-Goff *et al.*, 2012; Shinozaki *et al.*, 2015). The utility of proxy data in interpreting overwash (i.e. tsunami and storm inundation) deposits can be strengthened by constraining their spatial distribution in the modern environment (Pilarczyk *et al.*, 2011; Pham *et al.*, 2017; Kosciuch *et al.*, 2018). Such baseline studies provide a basis that anomalous sand layers, contained within the geological record, can be interpreted.

The spatial distributions of three proxies for palaeotsunami identification were examined and mapped at Hasunuma Beach in central Kujukuri (Fig. 1); foraminiferal taxonomy, foraminiferal taphonomy (i.e. surface character of individual tests) and sediment grain size. Although a multi-proxy approach is necessary to properly assess overwash deposits, determining which proxies are most useful for assessing sediment provenance is of particular importance because although this region was inundated by the 2011 Tohoku tsunami (Goto *et al.*, 2012), little is known about the long-term patterns of tsunami recurrence and magnitude. The establishment of a modern baseline study for palaeotsunami recognition and sediment provenance assessment will aid in the interpretation of older tsunami deposits preserved in coastal sediments in the region around Metropolitan Tokyo (Fujiwara & Kamataki, 2007).

SITE DESCRIPTION

Hasunuma Beach is part of the Kujukuri strand plain system located on the Pacific side of Japan *ca* 50 km east of Tokyo (Fig. 1A and B). The close proximity of the Kujukuri strand plain to the convergent boundaries between the Continental, Pacific Ocean and Philippine Sea plates has resulted in net tectonic uplift over the Holocene (e.g. Shishikura, 2000, 2001;

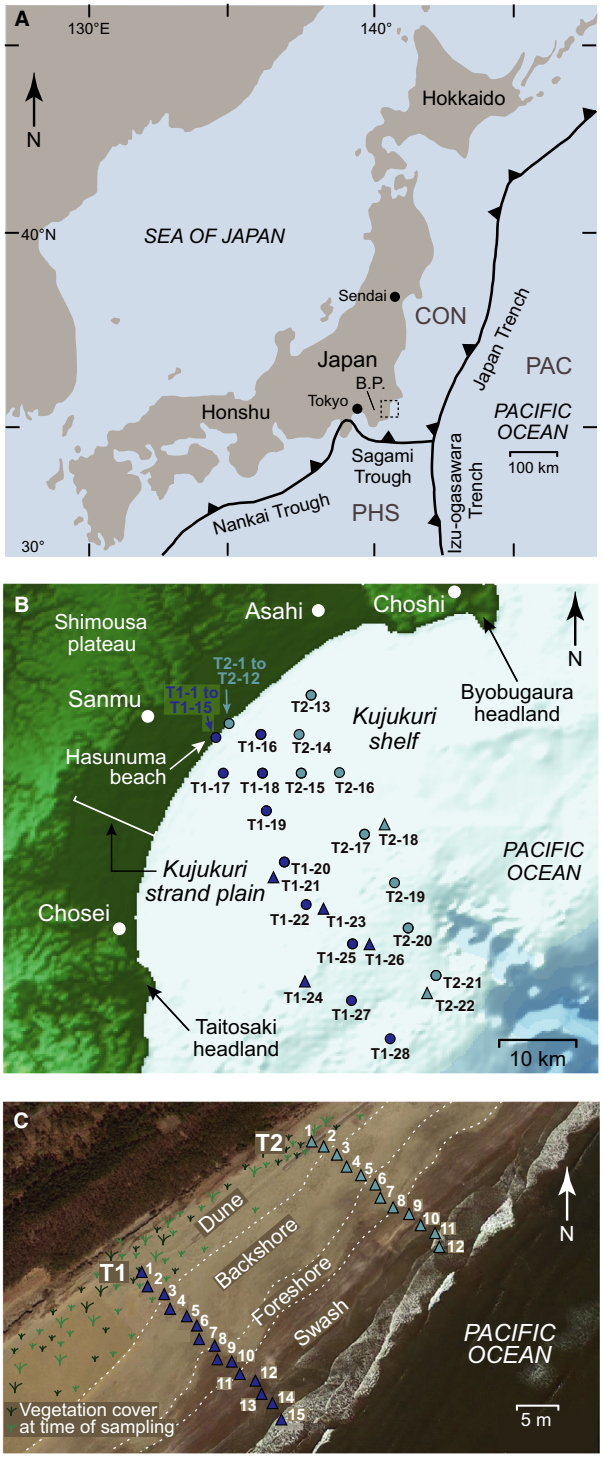

Fig. 1. (A) Location of the Kujukuri strand plain (square dotted outline) on the Boso Peninsula (B.P.) relative to broad-scale tectonics. Pacific (PAC), Philippine Sea (PHS) and Continental (CON) plates are indicated. (B) Map of the Kujukuri strand plain and Kujukuri shelf showing location of modern transects 1 (T1) and 2 (T2). Each transect has an onshore and offshore component. (C) Detailed map of the Hasunuma Beach shoreline indicating major geomorphological features and the location of surface samples collected from sub-environments within the coastal zone. Coloured triangles indicate samples that were stained with Rose Bengal.

Shishikura & Miyauchi, 2001; Tamura *et al.*, 2010). This net uplift, in combination with a continuous supply of sediment from eroding headlands, has permitted the formation of a prograding strand plain system that is 7 to 10 km wide and extends *ca* 50 km in a north-east/south-west direction (Shishikura, 2000). A series of parallel and subparallel sandy beach ridges (ranging in height from 2 to 10 m above TP; TP = Tokyo Peil, the mean sea-level at Tokyo Bay) and swales document a history of prograding shorelines over the last 6000 years (Moriwaki, 1979; Masuda *et al.*, 2001; Tamura *et al.*, 2007) to a maximum of 10 km in a seaward direction (Sunamura & Horikawa, 1977).

The landward limit of the Kujukuri strand plain is bounded by marine terraces composed of Pleistocene marine deposits and loam (Marine Isotope Stage 5e) that reach up to 130 m above TP in elevation (Tamura *et al.*, 2010). The seaward limit is characterized by a series of continuous sandy beaches (*ca* 100 to 200 m in width) along a microtidal (mean high tide level of 1·07 m above TP) coastline. The shelf offshore Kujukuri is characterized by a thin layer of Holocene sand and outcrop (Nishida *et al.*, 2019), leaving eroding headlands (e.g. Byobugaura & Taitosaki coastal cliffs) as the main sediment input to the coastal zone, with river discharge contributing a minor amount (Uda, 1989).

The coastal environment is divided into four broad zones according to elevation, distance from the shoreline and geomorphic features: (i) a shallow sloping sediment starved shelf (Kujukuri shelf) reaching depths up to 200 m; (ii) a high-energy, wave-dominated swash zone; (iii) a gently sloping beach face consisting of both foreshore and backshore zones (Tamura *et al.*, 2008); and (iv) a sparsely vegetated dune that transitions into a stable dune system characterized by shrubs, trees and tall grasses (Fig. 1C).

The position of the Kujukuri beaches relative to the open Pacific Ocean, as well as the Japan Trench and Sagami Trough, make the coastline vulnerable to inundation by tsunamis (for

example, the 2011 Tohoku tsunami; Matsumoto *et al.*, 2016) and typhoons. Notable coastal flooding events of varying magnitude that have impacted the Kujukuri beaches occurred in 1677 (Empo tsunami), 1703 (Genroku tsunami) and 2011 (Tohoku tsunami) (Namegaya *et al.*, 2011; Goto *et al.*, 2012).

METHODS

Sample collection and elevations

A total of 50 surface sediment samples (15 cm^3 from the upper 1 cm) were collected from two shore-perpendicular coastal transects (T1 and T2) near Hasunuma Beach, located in Central Kujukuri (Figs 1B, 2A and 3A) for grain-size and foraminiferal (taxonomy and taphonomy) analyses. Transects were positioned in areas that represent the full coastal gradient spanning the dune (*D*), backshore (*BS*), foreshore (*FS*), swash (*S*) and offshore (*O*) sub-environments (Fig. 1B and C). Sediments from each of these geomorphic zones were sampled along two transects (T1 and T2). Transects T1 and T2 are shore perpendicular transects consisting of 28 (T1-1 to T1-28; Fig. 2) and 22 samples (T2-1 to T2-22; Fig. 3), respectively (Tables S1 to S4).

A topographic survey was conducted with a Virtual Reference Station (VRS) using the Real Time Kinematic Global Positioning System (RTK–GPS) GS10 (Leica Geosystems Company Limited, Tokyo, Japan) with elevations tied to Tokyo Peil (m above TP). The survey was conducted at each sample location within the dune, backshore, foreshore and swash sub-environments; whereas a Crescent A100, VS110 GPS Compass (Hemisphere GPS Inc., Calgary, Canada), and Echo sounders PDR-1300 and PDR-130 (Senbondenki Company Limited, Tokyo, Japan) and JFE 380 (Japan Radio Company Limited, Tokyo, Japan) were used to measure the position and depth of all offshore samples.

The offshore samples span the entire Kujukuri shelf and were collected in 2014 and 2015 using a Smith-McIntyre grab sampler (upper 0 to 5 cm of surface sediment) deployed from a boat. Dune, backshore, foreshore and swash samples were collected in 2013 by means of a walking survey. Coastal transects were used to target the likely sources of overwash sediment for the purpose of establishing a detailed modern distribution that can be used for comparison with the palaeorecord by future studies. Sediment samples (15 cm^3 from the upper 1 cm) from each of the sub-environments were described in terms of grain-size and foraminiferal (taxonomy and taphonomy) content. Grain-size and foraminiferal data were then clustered using Partitioning Around Medoids (PAM) cluster analysis to discriminate biofacies, taphofacies, lithofacies and combination-facies.

Grain-size analysis

Grain-size analysis was conducted on 50 surface samples using a Camsizer (Retsch Technology GmbH, Haan, Germany; measuring grain sizes between 1·6 μm and 3200 μm). Prior to analysis on the Camsizer, organics and carbonates were removed using 30% hydrogen peroxide and 10% hydrochloric acid and dried at 50°C for 72 h (Matsumoto *et al.*, 2016). The average of three replicates was determined before converting grain-size values to the Wentworth-Phi Scale (Krumbein, 1934). Grain-size values and abundances for each transect were interpolated and gridded using a Triangular Irregular Network (TIN) algorithm according to Sambridge *et al.* (1995) and plotted as Particle-Size Distribution (PSD) plots in Geosoft Oasis TM (Figs 2B and 3B; Donato *et al.*, 2009). Grain-size descriptions follow that of Blott & Pye (2001). Statistical parameters including: mean (average grain size), mode (dominant grain size), standard deviation (degree of sorting), skewness (degree of symmetry of the grain-size distribution), kurtosis (peakedness of a grain-size distribution), and d10, d50 and d90 (grain size at which 10%, 50% or 90% of a sample's volume is occupied by smaller grains) were used to characterize each sample and are listed in Tables S1 and S2.

Foraminiferal analysis

Thirty-three surface sediment samples for foraminiferal analysis were stained with Rose Bengal and stored in buffered ethanol in the field immediately following collection to identify living versus dead individuals (Figs 2C and 3C; Walton, 1952; Murray & Bowser, 2000). An additional 17 unstained surface sediment samples were used where only the total assemblage was considered. Prior to analysis, 10 cm^3 sediment samples were washed over a 63 μm sieve and the sample was wet split to obtain counts of *ca* 300 specimens (Scott & Hermelin, 1993). The

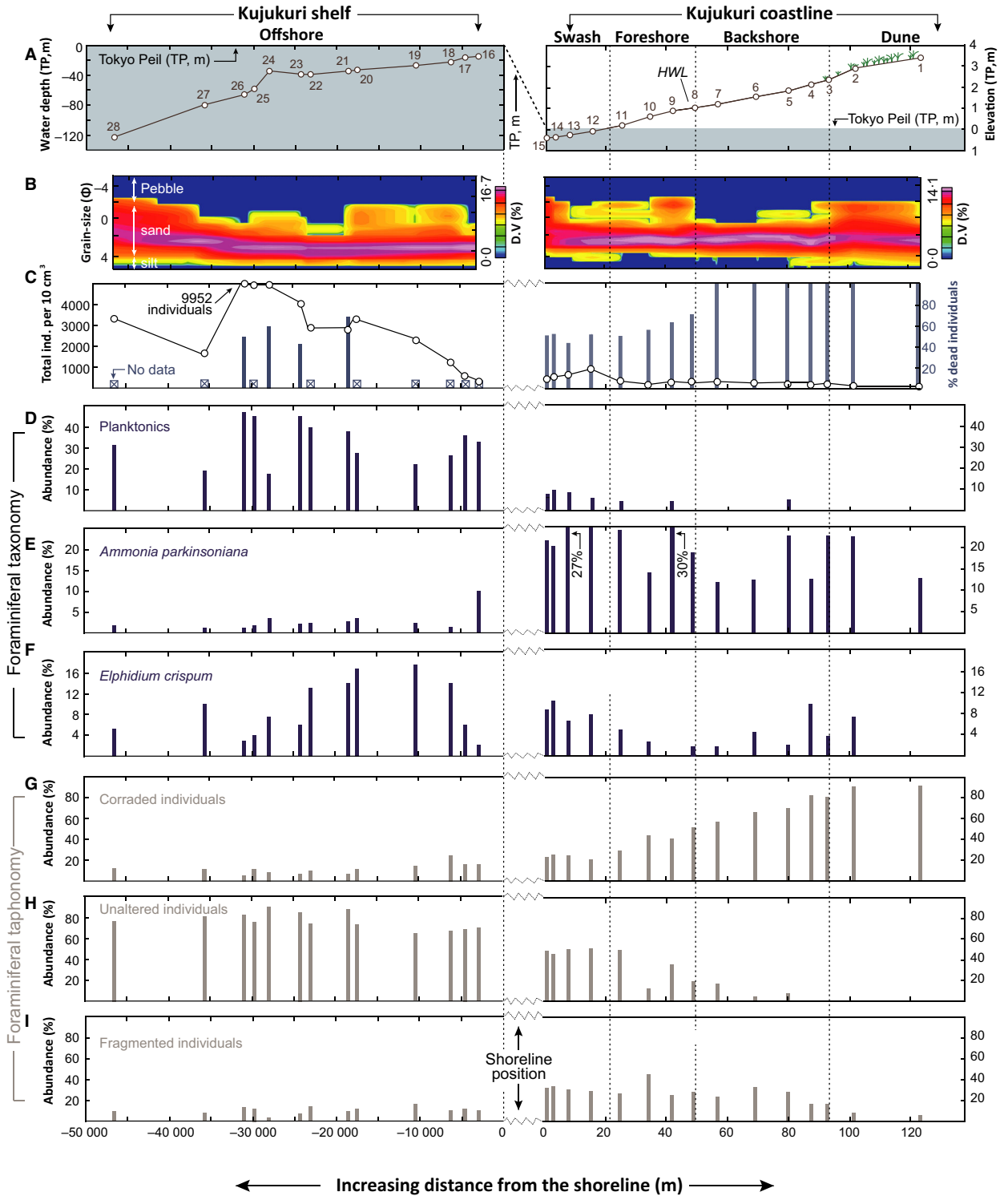

Fig. 2. T1 surface samples. (A) Elevation profile extending from the offshore zone of the Kujukuri shelf to the dunes of Hasunuma Beach using the Tokyo Peil datum (TP; mean sea-level in Tokyo Bay). (B) Particle-size distribution (PSD) plot for T1 reported as differential volume (D.V.) percent. The relative proportion (i.e. D.V. percent) of sample within each grain-size interval measured by the Camsizer [between −5 Φ (pebble) and 5 Φ (silt)] is plotted against distance from the shoreline. (C) to (F) Total individuals per 10 cm^3, relative abundances of dead individuals and dominant foraminiferal taxa. (G) to (I) Relative abundances of foraminiferal taphonomic (i.e. test surface condition) data.

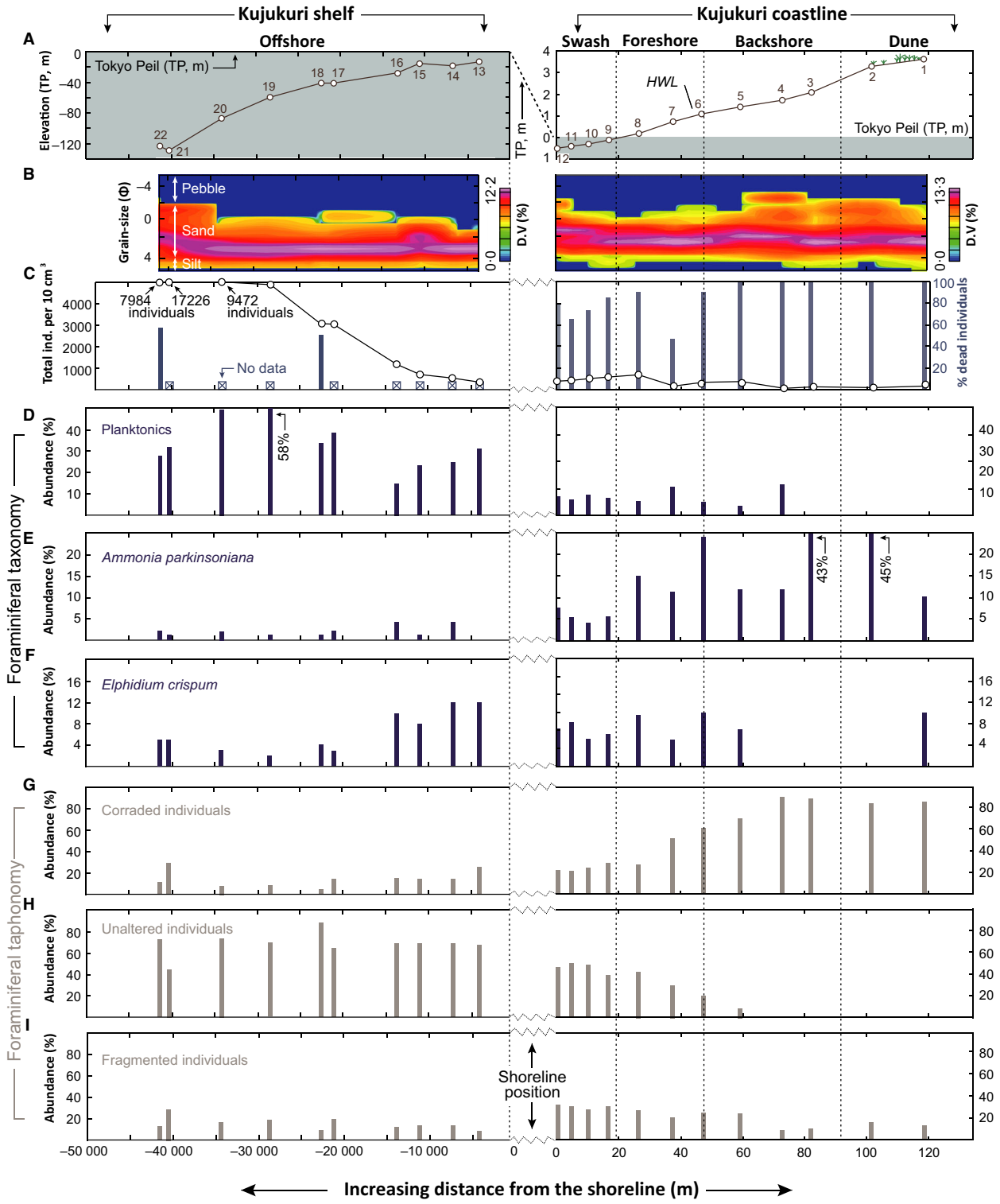

Fig. 3. T2 surface samples. (A) Elevation profile extending from the offshore zone of the Kujukuri shelf to the dunes of Hasunuma Beach using the Tokyo Peil datum (TP; mean sea-level in Tokyo Bay). (B) Particle-size distribution (PSD) plot for T2 reported as differential volume (D.V.) percent. The relative proportion (i.e. D.V. percent) of sample within each grain-size interval measured by the Camsizer [between −5 Φ (pebble) and 5 Φ (silt)] is plotted against distance from the shoreline. (C) to (F) Total individuals per 10 cm^3, relative abundances of dead individuals and dominant foraminiferal taxa. (G) to (I) Relative abundances of foraminiferal taphonomic (i.e. test surface condition) data.

total number of foraminifera (living and dead) contained within 10 cm^3 was calculated for each sample site (Figs 2C and 3C; Tables S3 and S4). Foraminiferal taxonomy followed Loeblich & Tappan (1987) and Uchida *et al.* (2010), and identifications were confirmed using the type specimens at the Smithsonian Institution in Washington DC. Figure 4 shows scanning electron microscope (SEM) images obtained using a Hitachi TM3030 tabletop microscope (Hitachi High-Tech, Fukoka, Japan) of the dominant foraminiferal taxa identified in this study.

Foraminifera were categorized using the same taphonomic criteria defined by Pilarczyk *et al.* (2011) which includes: unaltered, fragmented and corraded (combined influence of corrosion and abrasion) individuals. Broken specimens with angular edges were classified as fragmented, whereas broken specimens with rounded edges were classified as corraded. The taphonomic (or surface) condition of individual foraminifera has previously been used to interpret overwash deposits because it is an indicator of the origin and transport history of the sediment (e.g. Goff *et al.*, 2011; Pilarczyk *et al.*, 2012; Hoffmann *et al.*, 2018). Elevation or depth (m above TP), total foraminifera in 10 cm^3, abundance (%) of dead (unstained) individuals (where available), dominant species and taphonomic character were plotted against increasing distance from the shoreline for both transects (Figs 2 and 3). Foraminiferal results are listed in Tables S3 and S4.

Cluster analysis

Partitioning Around Medoids cluster analysis was used to objectively determine biofacies, taphofacies, lithofacies and combination-facies that were then compared with observed geomorphic beach zones along transects T1 and T2. Prior to cluster analysis taxonomic, taphonomic and grain-size values were standardized; first, raw counts (taxonomic and taphonomic data) and measurements (grain-size data) were converted to abundances (%), and then Z-scores were calculated and used for clustering. The Z-scores are a means of standardizing datasets by assessing how many standard deviations a value is from the mean (Davis & Sampson, 2002). The PAM cluster analysis (Kaufman & Rousseeuw, 1990) was then performed following the methods of Kemp *et al.* (2012), where the 'cluster' package in R (Maechler *et al.*, 2005) was used to identify zonation within the Kujukuri coastal transect based on combinations of foraminiferal taxonomy (total assemblage), taphonomy and grain-size datasets.

Partitioning Around Medoids (PAM) generates silhouette plots with widths ranging from −1 to 1. Silhouettes are an estimate of a sample's classification where values close to −1 are those that are incorrectly classified; whereas values close to 1 indicate that the sample was assigned to the appropriate cluster. The maximum average silhouette width was used to objectively determine the number of clusters within each dataset combination of this study (for example, tests 1 to 7; see below). Methods for determining silhouette width are detailed in Kaufman & Rousseeuw (1990).

In order to determine which datasets clustered most effectively, seven combinations of data were clustered using % abundances: *test 1* (taxonomy); *test 2* (taphonomy); *test 3* (grain size); *test 4* (taxonomy and taphonomy); *test 5* (taxonomy, taphonomy and grain size); *test 6* (taxonomy and grain size); and *test 7* (taphonomy and grain size). These tests were performed on T1 (Figs S1 to S3) and T2 (Figs S4 to S6) separately to determine the spatial variability at Hasunuma Beach, and then the datasets were combined (T1 and T2; Figs 5 and S7 to S10) to determine regional variability.

RESULTS

Grain size

Transect 1 (T1)

Average (mean) grain size. Transect T1 spanned a distance of 47 km from the coastal dunes of Hasunuma Beach (3·4 m above TP) to the seaward edge of the Kujukuri shelf (−123 m above TP). The mean grain size along this transect ranged from fine to coarse sand, with all but two samples (T1-15 and T1-28) in the fine to medium sand range (Fig. 2B; Table S1). In general, the mean grain size became finer with depth, with sediments from the dune (average mean = 1·98 Φ), backshore (average mean = 1·94 Φ) and foreshore (average mean = 1·92 Φ) being slightly coarser than those from the offshore (average mean = 2·50 Φ). The one exception to this seaward fining trend was the swash zone, where the average mean grain size was 1·45 Φ. Within the offshore zone, sediments became progressively finer with increased distance from the shoreline up to a distance of 23 km (for example, 2·70 Φ at T1-16 versus 2·97 at T1-22), at which point the sediments became

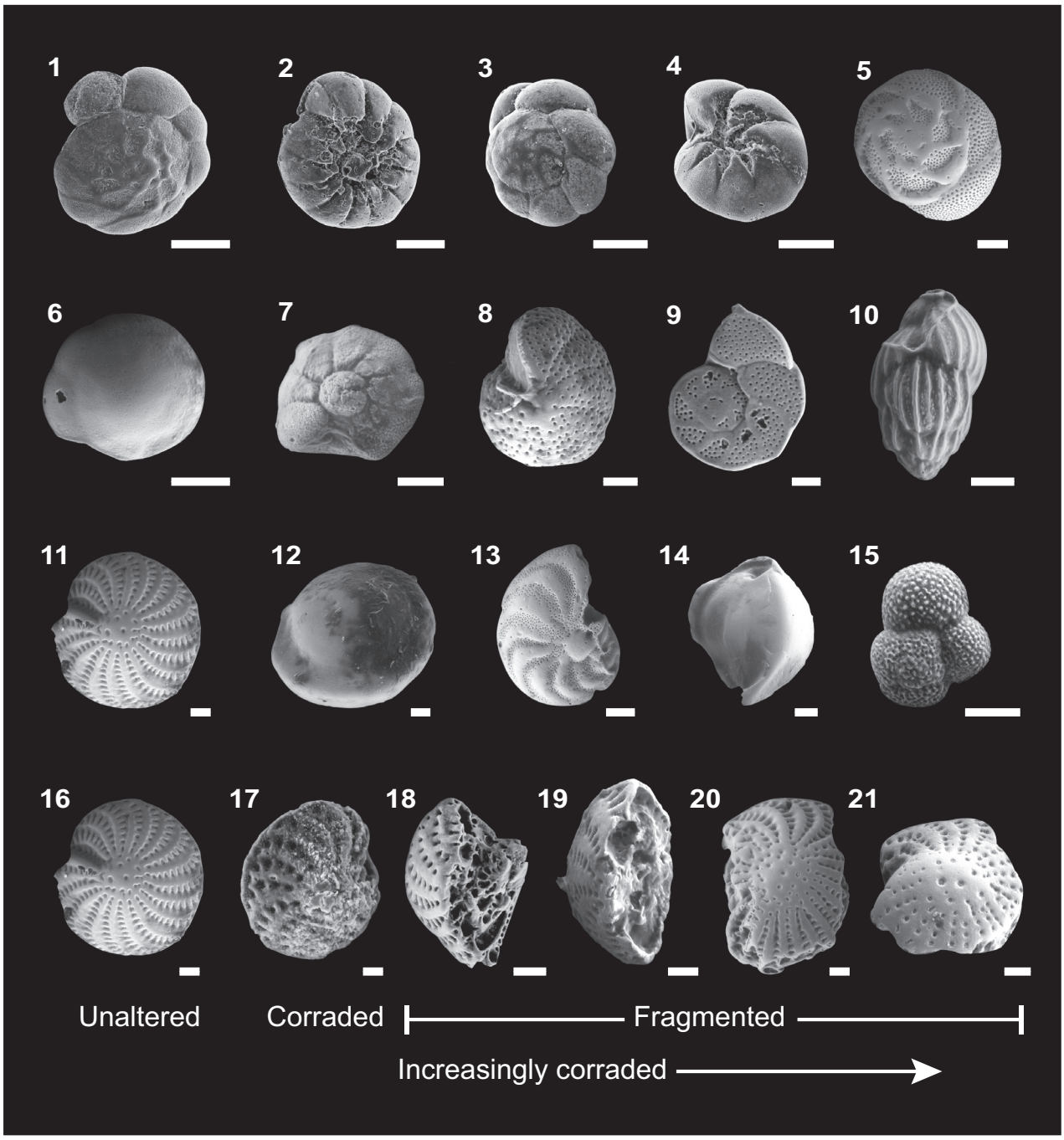

Fig. 4. Scanning electron microscope (SEM) images of dominant foraminiferal taxa and taphonomic states. All scale bars are equal to 100 μm. (1) and (2) *Ammonia parkinsoniana*, (3) and (4) *Ammonia tepida*, (5) *Buccella frigida*, (6) and (7) *Pararotalia nipponica*, (8) and (9) *Cibicides reflugens*, (10) *Uvigerina* spp., (11) *Elphidium crispum*, (12) *Lenticulina* sp., (13) *Anomalinidae* sp., (14) *Quinqueloculina* spp., (15) Planktonic. Taphonomic states of *Elphidium crispum*: unaltered (16), corraded (17) to (21), and fragmented (18) to (21) individuals.

progressively coarser (for example, 2·81 Φ at T1-23 versus 0·155 Φ at T1-28).

Dominant grain size (mode). The average mode, or dominant grain size within a given distribution, became finer with increasing distance inland from the swash (for example, average mode in dune samples = 2·05 Φ versus 1·76 Φ in the swash). In general, the finest mode values were found in the offshore samples,

which showed progressive fining up to a distance of 23 km from the shoreline (for example, 2·62 Φ at T1-16 versus 3·12 Φ at T1-22), at which point the mode became progressively coarser (2·88 Φ at T1-23 versus 1·12 Φ at T1-28).

Degree of sorting. Aside from the two coarsest samples, T1-15 and T1-28, which were poorly sorted (1·08 Φ and 1·25 Φ, respectively), sediment along T1 was moderately to very well-sorted (0·81 Φ to 0·32 Φ; Table S1). In general, the degree of sorting increased in a seaward direction from the dune (moderately well-sorted; average SD = 0·60 Φ) to the offshore (well-sorted; average SD = 0·45 Φ). However, with an average degree of sorting of 0·80 Φ (moderately sorted), the swash was the least sorted zone.

Skewness and kurtosis. In general, most samples from T1 had a symmetrical grain-size distribution and mesokurtic kurtosis (sediment profile curve with a normal distribution). Coarsely skewed (sediment profile curve where the coarse grains dominate) samples were generally limited to the offshore zone, with T1-11 in the foreshore and T1-4 in the backshore also exhibiting coarse skewness (−0·11 Φ and −0·12 Φ, respectively). The only finely skewed (sediment profile curve where the fine grains dominate) sample was T1-15 collected from the swash zone (0·10 Φ). Platykurtic (a sediment profile curve that is wider around the mean and has a thin tail) samples were exclusive to the foreshore and swash zones, where sediments were generally the coarsest (mean grain size = 1·80 to 1·57 Φ) and the least sorted (mean SD = 0·81 to 0·65 Φ). The one exception to this pattern was T1-28, a poorly sorted coarse sand with a platykurtic kurtosis of 0·81 Φ. By contrast, samples with leptokurtic kurtosis (sediment profile curve that is more clustered around the mean and has fatter tails) were only found in the offshore zone, with seven of the 13 samples collected from the offshore containing this type of kurtosis.

Transect 2 (T2)

Average (mean) grain size. Transect T2 spanned a distance of 41 km from the coastal dunes of Hasunuma Beach (3·6 m above TP) to the seaward edge of the Kujukuri shelf (−124 m above TP). The mean grain size along this transect ranged from fine to coarse sand, with all but one sample (T2-21) in the fine to medium sand range (Fig. 2B; Table S2). Similar to T1, the mean grain size along T2 became finer with depth. Sediments from the dune (average mean = 1·96 Φ), backshore (average mean = 1·76 Φ), and foreshore (average mean = 1·89 Φ) were slightly coarser than those from the offshore (average mean = 2·32 Φ). The coarsest samples were from the swash zone, where the average mean grain size was 1·34 Φ). Within the offshore zone, sediments were generally within range of fine sand (2·80 to 1·95 Φ) until a distance of 40 km, at which point the sediments increased in grain size (for example, 2·63 Φ at T2-20 versus 0·87 Φ at T2-21).

Dominant grain size (mode). The dominant grain size along T2 did not show a fining trend as strong with increasing distance in a seaward direction as T1. Although the coarsest modes were found in the swash zone (average mode = 1·15 Φ), the foreshore samples were generally finer (average mode = 2·05 Φ) than the dune samples (average mode = 1·96 Φ). Similar to T1, the finest mode values were found in the offshore samples up to a distance of 34 km (2·87 to 2·37 Φ), at which point the mode became increasingly coarser (2·37 Φ at T2-20 versus 1·62 Φ at T2-22).

Degree of sorting. The most poorly sorted samples from T2 were T2-21 (1·48 Φ) and T2-22 (1·13 Φ) at the edge of the Kujukuri shelf. Similar to T1, all other samples were moderately to well-sorted (0·85 Φ to 0·35 Φ; Table S2). In general, the degree of sorting was relatively consistent within dune (moderately well-sorted; average SD = 0·58 Φ), backshore (moderately well-sorted; average SD = 0·62 Φ), foreshore (moderately well-sorted; average SD = 0·59 Φ) and offshore sediments (moderately well-sorted; average SD = 0·63 Φ), with swash sediments being the least sorted (moderately sorted; average SD = 0·74 Φ).

Skewness and kurtosis. In general, similar to T1, most samples from T2 had a symmetrical grain-size distribution and mesokurtic kurtosis. Coarsely and very coarsely skewed sediments were limited to the foreshore and offshore zones. Finely skewed samples were found in the swash zone at T2-10 to T2-12 (0·26, 0·26 and 0·25 Φ, respectively), with one anomalous finely skewed sample within the backshore (0·10 Φ at T2-4). Platykurtic samples were generally found only in the swash zone (for example, T2-12, T2-11 and T2-9), although T2-15 also had a platykurtic kurtosis (0·77 Φ).

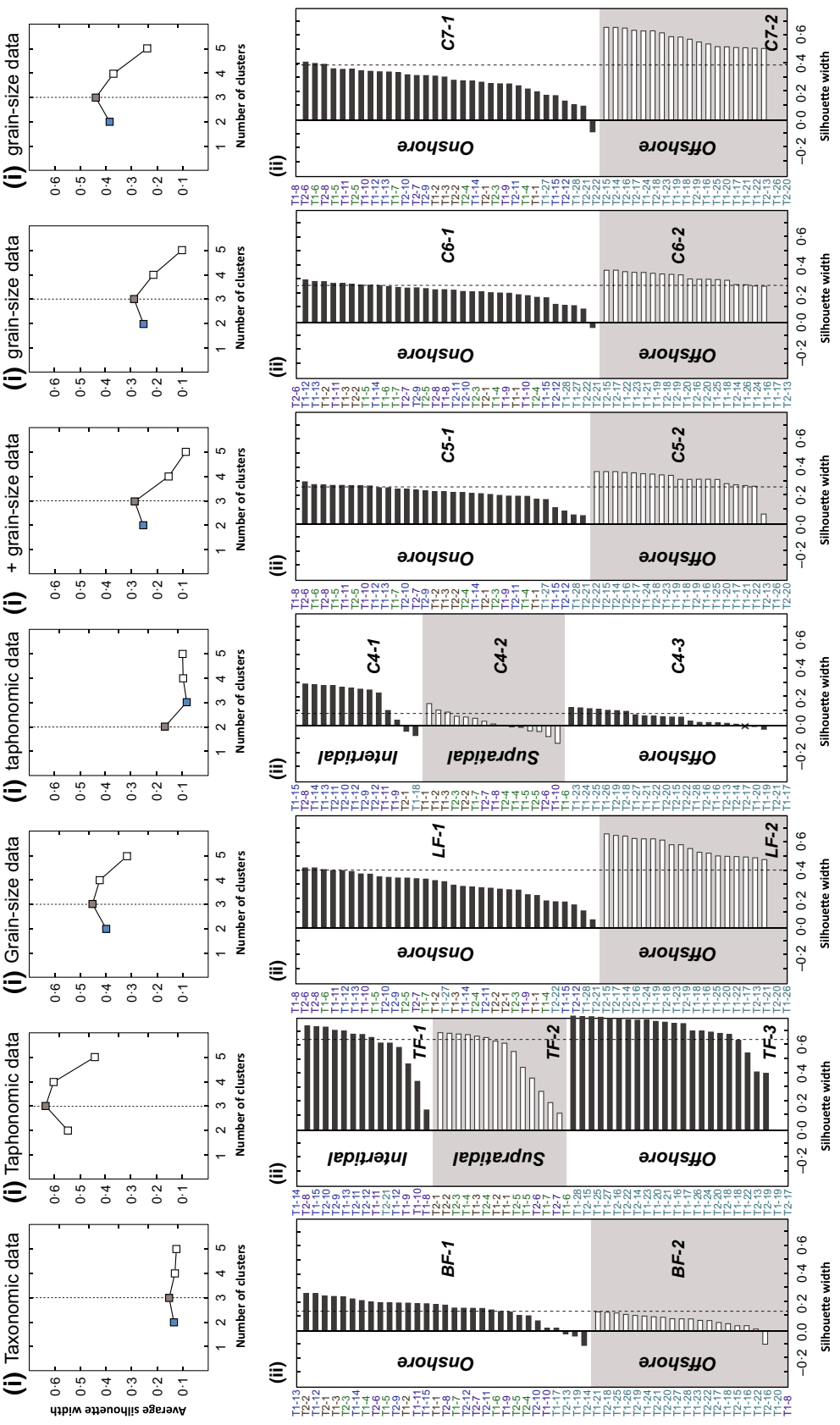

Observed coastal zone:

T1-1 - T1-3, T2-1 - T2-2...dune *T1-4 - T1-7, T2-3 - T2-5...backshore* *T1-8 - T1-11, T2-6 - T2-8...foreshore*

T1-12 - T1-15, T2-9 - T2-12...swash *T1-16 - T1-28, T2-13 - T2-22...offshore*

Fig. 5. Results of Partitioning Around Medoids (PAM) cluster analysis for tests 1 to 7 (A) to (G) indicating average silhouette width of clustered data involving 2, 3, 4 and 5 clusters (i). For tests 1, 3 and 5 to 7, the two-cluster scenario produced either the highest average silhouette width (dashed line) or the greatest number of samples assigned to the appropriate cluster, indicating that the data in each test can be reliably divided into two facies (BF = biofacies; TF = taphofacies; LF = lithofacies; C4 = test four clusters; C7 = test seven clusters). For tests 2 and 4, the three-cluster scenario grouped samples into offshore, intertidal, and supratidal groupings. Silhouette plots for tests 1 to 7 divided into two or three groups are shown in (ii)

Samples with leptokurtic kurtosis were only found in the offshore zone, with seven of the ten samples collected from the offshore containing this type of kurtosis.

Foraminifera

Transect 1 (T1)

Foraminifera are present in all samples retrieved from T1 (Fig. 2; Table S3). Moving from the dune to the offshore, the total concentration of foraminifera ranged from 10 to 9952 individuals per 10 cm^3. Concentrations of foraminifera peaked in the offshore zone (320 to 9952 individuals per 10 cm^3) and markedly decreased in the swash zone (382 to 956 individuals per 10 cm^3), foreshore (68 to 240 individuals per 10 cm^3), backshore (74 to 86 individuals per 10 cm^3) and dune (10 to 42 individuals per 10 cm^3).

A total of 23 foraminiferal species were present in T1 samples. The offshore zone is dominated by planktonics (17 to 48%); the swash zone by *Pararotalia nipponica* (28 to 33%), *Ammonia parkinsoniana* (22 to 27%) and *Elphidium crispum* (7 to 11%); the foreshore by *P. nipponica* (27 to 35%), *A. parkinsoniana* (15 to 30%) and *Anomalinidae* sp. (4 to 15%); the backshore by *P. nipponica* (27 to 47%), *A. parkinsoniana* (12 to 23%) and *Cibicides reflugens* (3 to 19%); and the dune by *P. nipponica* (35 to 53%) and *A. parkinsoniana* (13 to 23%). Planktonic species are present in moderate abundances throughout most of T1 (0 to 48%) but are generally only found in sediments up to a distance of *ca* 40 m inland.

The taphonomic condition of foraminifera contained within sediments from T1 includes fragmented, abraded and unaltered forms. Samples within the swash zone are exclusively dominated by unaltered individuals (44 to 52%); whereas samples within the foreshore, backshore and dune are generally dominated by corraded individuals (27 to 51%, 58 to 82% and 81 to 93%, respectively). By contrast, offshore samples were dominated by unaltered individuals (65 to 88%).

Transect 2 (T2)

Foraminiferal concentrations contained within T2 sediments are similar to those observed from T1 (Fig. 3; Table S4). Concentrations of foraminifera were highest in the offshore zone (256 to 17 216 individuals per 10 cm^3), followed by the swash (358 to 594 individuals per 10 cm^3), foreshore (34 to 668 individuals per 10 cm^3), backshore (16 to 82 individuals per 10 cm^3) and dune (22 to 38 individuals per 10 cm^3).

Dominant species within the assemblages at T2 showed minor variations when compared with T1 assemblages. The offshore zone is dominated by planktonics (15 to 58%); the swash by *P. nipponica* (38 to 48%), *E. crispum* (5 to 8%) and planktonic species (6 to 9%); the foreshore by *P. nipponica* (34 to 44%), *A. parkinsoniana* (12 to 24%) and *C. reflugens* (7 to 18%); the backshore (BS) and dune (D) by *P. nipponica* (BS = 37 to 50%; D = 54 to 63%) and *A. parkinsoniana* (BS = 12 to 43%; D = 10 to 45%). Planktonics are present (4 to 58% of the assemblage) up to a distance of 70 m inland.

Similar to T1, the offshore (O) and swash (S) zones are characterized by high abundances of unaltered individuals (O = 45 to 86%, S = 39 to 49%), whereas, the foreshore, backshore and dune are dominated by corraded individuals (27 to 60%, 71 to 87% and 82 to 84%, respectively).

Cluster analysis: biofacies, taphofacies and lithofacies

Datasets from T1 (Figs S1 to S3) and T2 (Figs S4 to S6) were first considered separately to examine spatial variability within the proxy data at Hasunuma Beach. The datasets (T1 + T2) were then combined to test whether coastal zones could be discriminated (Figs S7 to S10). In the case of T1 versus T2, tests that produced the highest average silhouette width were ordered in the same way (Table 1), with *test 2* (taphonomy; T1 = 0·56, T2 = 0·48; Figs S1b*i* and S4b*i*, respectively) and *test 3* (grain size; T1 = 0·41, T2 = 0·40; Figs S1c*i* and S4c*i*, respectively) producing the greatest widths, and *test 1* (taxonomy; T1 = 0·16, T2 = 0·12; Figs S1a*i* and S4a*i*, respectively) producing the smallest widths. All seven tests for each of T1 and T2 indicate that the data can be reliably divided into two to three clusters. For T2 *test 1*, the five-cluster scenario produced the highest average silhouette width (0·14), but one of the clusters returned a value of 0, indicating that it was composed of a single sample (Fig. S4a*v*). This is similar to T2 *test 3*, where the four-cluster scenario also retuned a 0 value for one of its clusters (Fig. S4c*iv*).

When considering T1 and T2 datasets collectively, PAM recognized two clusters (onshore and offshore clusters) for each of the seven tests, except for *test 2* (taphonomy) which recognized three clusters (supratidal, intertidal and offshore clusters) (Fig. 4). Ordered from highest silhouette

Table 1. Highest average silhouette width for tests 1 to 7. Results for transect 1 (T1), transect 2 (T2) and transects 1 and 2 combined (T1 + T2) for two to five cluster-scenarios. Highest silhouette widths per cluster scenario are indicated in bold.

	Two-cluster scenario			Three-cluster scenario			Four-cluster scenario			Five-cluster scenario		
Transect No.	T1	T2	T1 + T2	T1	T2	T1 + T2	T1	T2	T1 + T2	T1	T2	T1 + T2
Test 1	**0·16**	0·12	0·13	**0·17**	0·13	0·16	0·11	**0·12**	**0·12**	0·13	**0·14**	0·11
Test 2	**0·56**	0·48	0·53	0·60	**0·67**	0·63	0·59	**0·64**	0·60	**0·61**	0·52	0·45
Test 3	**0·41**	0·40	0·40	**0·49**	0·39	0·46	**0·46**	0·41	0·42	**0·44**	0·37	0·31
Test 4	**0·19**	0·16	0·18	0·10	**0·16**	0·08	0·12	**0·15**	0·10	**0·15**	**0·15**	0·10
Test 5	**0·27**	0·25	0·26	**0·31**	0·23	0·29	**0·19**	0·15	0·16	**0·17**	0·12	0·09
Test 6	**0·27**	0·25	0·26	**0·31**	0·22	0·29	**0·27**	0·15	0·21	**0·18**	0·11	0·10
Test 7	**0·40**	0·38	0·39	**0·48**	0·39	0·44	0·33	0·33	**0·37**	0·30	**0·33**	0·24

width to the lowest, the T1 + T2 dataset produced the same order as T1 and T2 individually (Table 1), with *test 2* (taphonomy; T1 + T2 = 0·53) and *test 3* (grain size; T1 + T2 = 0·40) producing the highest silhouette widths, and *test 1* producing the lowest (taxonomy; T1 + T2 = 0·13). Cluster analysis on combined proxy datasets produced silhouette widths that were generally less than those obtained from individual datasets: *test 7* (average silhouette width = 0·39); *test 6* (average silhouette width = 0·26); *test 5* (average silhouette width = 0·26); and *test 4* (average silhouette width = 0·18).

In six of the seven tests, the highest average silhouette width was produced by the three-cluster scenario (all tests except *test 4*). However, only in the case of *test 2* (taphonomy) did the clusters make ecological sense (average silhouette width = 0·46; 94% of samples clustered in the appropriate group). Taphonomy strengthened taxonomic data. For example, under the two-cluster scenario, taxonomy had an average silhouette width of 0·13 and 90% of samples clustered in the appropriate group, while taxonomy and taphonomy had an average silhouette width of 0·18 and 98% of samples clustered appropriately. Taphonomy did not improve grain size; the accuracy of clustered samples remained the same (90%) and the average silhouette width only varied by 0·01 (Table 1). Adding all three parameters together did not improve the accuracy of appropriately clustered samples or the average silhouette width by much, except in the case of taxonomy.

Following cluster analysis on the combined dataset (T1 + T2), PAM defined clusters were used to describe biofacies (*test 1*, taxonomy), taphofacies (*test 2*, taphonomy) and lithofacies (*test 3*, grain size), as well as facies resulting from the various combinations of datasets (C4, C5, C6 and C7; Fig. 5).

Biofacies (test 1)

Group BF-1 (onshore group) has an average silhouette width of 0·16 and is dominated by *Pararotalia nipponica* (9 to 63%). The elevation of this cluster ranges from −34 to 4 m above TP, and its distance from the shoreline ranges from −18 460 to 120 m. Group BF-2 (offshore group) has an average silhouette with of 0·08. The elevation of samples in BF-2 ranges from −124 to 1·0 m above TP, and their distance from the shoreline ranges from −46 600 to 49 m. The foraminiferal assemblage of BF-2 is characterized by low abundances of fragile tested species including: *Uvigerinella glabra*, *Bucella frigida* and *A. tepida*.

Taphofacies (test 2)

Group TF-1 (intertidal group) is characterized by an average silhouette width of 0·61, an elevation of −0·5 to 1·0 m above TP and a distance from the shoreline of 0 to 49 m. The taphonomic assemblage of TF-1 is dominated by unaltered foraminifera (12 to 52%), followed by fragmented foraminifera (25 to 44%) and corraded foraminifera (20 to 44%). Group TF-2 (supratidal group) had an average silhouette width of 0·53, an elevation of 0·7 to 3·6 m above TP, and a distance from the shoreline ranging from 40 to 120 m. Unlike TF-1, TF-2 is dominated by corraded individuals (53 to 93%), followed by those that were fragmented (7 to 32%) and unaltered (0 to 29%). Group TF-3 (offshore group) is characterized by an average silhouette width of 0·72, an elevation of −125 to −13 m above TP, and a distance from the shoreline of −3080 to −46 600 m. Group TF-3 is dominated by

planktonic species (15 to 58%) and individuals that are dominantly unaltered (64 to 88%).

Lithofacies (test 3)

Group LF-1 (onshore group) has an average silhouette width of 0·31, and samples within the cluster range in elevation from −124 to 4 m above TP, and −46 600 to 123 m in distance from the shoreline. Samples within LF-1 have a mean grain size of 0·15 to 2·15 ϕ (coarse to medium sand), with fine sand being the dominant grain size (d90 = 1·61 to 2·95 ϕ). Group LF-2 (offshore group; average silhouette width = 0·58) is dominated by samples that are slightly finer (mean = 2·57 to 2·97 ϕ, d90 = 3·05 to 3·40 ϕ) but still in the medium sand range. Samples from LF-2 are characterized elevations that range from −87 to −13 m above TP and distances from the shoreline that range from −3080 to −33 640 m (excluding T1-12 that clustered erroneously).

Combination facies (tests 4 to 7)

Combination facies described here consist of those from *test 4* (C4-1 to C4-3), *test 5* (C5-1, C5-2), *test 6* (C6-1, C6-2) and *test 7* (C7-1, C7-2; Figs 5 and S8 to S10) and will be discussed in order of highest to lowest average silhouette width.

Sample locations within C7-1 range in elevation from −124 to 4 m above TP and range between 123 m and −46 600 m from the shoreline. Unaltered foraminifera dominate the taphonomic assemblage in 45% of the samples from this cluster. The C7-1 cluster is characterized by sediments that are generally in the medium sand range (average mean grain size = 1·68 ϕ) but range from 0·15 (coarse sand) to 2·15 ϕ (fine sand). The d90 of samples within this cluster remains relatively constant within the medium sand range (1·61 to 2·95 ϕ); however, the d10 fluctuates between very fine pebbles (−1·37 ϕ) and medium sand (1·56 ϕ). The C7-2 cluster contained samples that were generally from lower elevations (−13 to −87 m above TP) and greater distances from the shoreline (−33 640 to −3808 m above TP) compared to those from C7-1. The sediment grain size of C7-2 was slightly finer than that of C7-1 (average mean grain size = 2·75 ϕ; fine sand), ranging from 2·57 to 2·97 ϕ (fine sand). Neither the d10 nor the d90 fluctuated beyond medium to fine (1·92 to 2·53 ϕ) and very fine (3·05 to 3·40 ϕ) sand, respectively.

The C6-1 cluster contains sample sites located between 123 m and −46 600 m from the shoreline and between −124 m and 4 m above TP in elevation. The C6-1 samples are generally dominated by *P. nipponica* (2 to 63%) and, in most cases, *A. parkinsoniana* (1 to 45%), with *C. refulgens* and *E. crispum* present in smaller abundances (<23%). The mean grain size ranges from coarse (0·15 ϕ) to fine (2·15 ϕ) sand and has an average mean grain size of 1·68 ϕ (medium sand). The d90 values are predominantly within the fine sand range; however, the d10 values fluctuate between medium (1·92 ϕ) and fine (2·53 ϕ) sand. Cluster C6-2 is comprised of offshore samples that are generally deeper (−13 to −87 m above TP) and further from the shoreline (−3080 to −31 140 m). Planktonics (15 to 58%) dominate the foraminiferal assemblage in these samples. The C6-2 samples are finer than those that clustered in C-1; the mean grain size ranges from 2·57 to 2·97 ϕ fine sand.

Test 5, which clusters all three datasets, defined two clusters that can be differentiated by their elevation and distance from the shoreline. Cluster C5-1 consists of samples that are within 123 m of the shoreline and between −0·5 to 4·0 m above TP, except for offshore samples T1-27, T1-28 and T2-21, T2-22. The dominant species within C5-1 samples are *P. nipponica* (3 to 63%), *A. parkinsoniana* (1 to 45%) and *E. crispum* (up to 11%), with most foraminifera categorized as either corraded (12 to 93%) or unaltered (0 to 81%). The mean grain size ranges from coarse (0·15 ϕ) to fine (2·15 ϕ) sand and has an average mean grain size of 1·64 ϕ (medium sand). The d90 values are all within the fine sand range (1·61 to 2·76 ϕ); however, the d10 values fluctuate between very fine pebbles (−1·67 ϕ) and medium sand (1·56 ϕ). The C5-2 samples were generally lower in elevation (−13 to −87 m above TP) and further from the shoreline (−3080 to −33 640 m) than those within the C5-1 cluster. *Pararotalia nipponica* and planktonics dominate the species assemblage, ranging from 3 to 19% and 15 to 58%, respectively. All samples that clustered in C5-2 contained a taphonomic assemblage that was dominated by unaltered individuals (64 to 88%). The sediment grain size of C5-2 was slightly finer than that from C5-1; the mean grain size ranges from medium (1·95 ϕ) to fine (2·97 ϕ) sand, with an average mean of 2·71 ϕ (fine sand). Neither the d10 or the d90 fluctuated beyond medium to fine (1·92 to 2·53 ϕ) and very fine (3·05 to 3·40 ϕ) sand, respectively, with the exception of T2-15.

Test 4 discriminated between intertidal (C4-1), supratidal (C4-2) and offshore (C4-3) samples. Cluster C4-1 consists predominantly (except for one offshore sample, T1-18) of swash and foreshore samples (elevation range = −0·5 to 4·0 m above TP) that are within 118 m of the shoreline. This cluster is largely defined by high abundances of *P. nipponica* (27 to 63%), *A. parkinsoniana* (4 to 30%) and *E. crispum* (0 to 11%), and is dominated by unaltered individuals (36 to 52%). Cluster C4-2 consists of sample locations that are further inland of the shoreline (34 to 123 m) and generally higher in elevation (0·6 to 4 m above TP). The C4-2 cluster is defined by high abundances of corraded individuals (44 to 93%). Similar to C4-1, C4-2 samples are dominated by *P. nipponica* (27 to 54%) and *A. parkinsoniana* (12 to 45%). Cluster C4-3 consists of samples collected from the offshore, ranging in distance from −3080 to −46 600 m from the shoreline and depths of −13 to −129 m above TP. Cluster C4-3 is dominated by planktonics (15 to 58%) and the highest abundances of unaltered specimens (45 to 88%).

DISCUSSION

Modern proxy distributions

Grain-size results are distinguished between onshore and offshore samples along two transects (Fig. 5). In general, the mean grain size along T1 and T2 ranged from fine to coarse sand and became progressively finer with increasing depth (Fig. 2), a trend previously documented along the Kujukuri shelf (Nishida *et al.*, 2019) as well as other locations (e.g. Gao & Collins, 1994). At a distance of *ca* 23 km offshore, the mean grain size became coarser, likely because of interaction with the Kuroshiro Current (Mizuno & White, 1983). Onshore samples were moderately well-sorted, which is to be expected because of wind-transported sediment accumulating in the dunes and sorting by waves and tides (Jiang *et al.*, 2015). Similarly, offshore samples were generally well-sorted to very well-sorted because sedimentation at these depths is a function of finer sediment settling out of suspension.

Taxonomic assemblages of foraminifera are often employed as a means of assessing both storm and tsunami deposits on the basis that marine taxa are transported inland to locations where they normally would not occur (e.g. Mamo *et al.*, 2009; Hawkes & Horton, 2012; Pilarczyk *et al.*, 2014). Studies have also used foraminifera to infer provenance of sediments contained within overwash sediments (Nanayama & Shigeno, 2006; Lane *et al.*, 2011; Hawkes & Horton, 2012; Sieh *et al.*, 2015). Even though numerous studies have reported on the distribution of foraminifera within nearshore and offshore environments (e.g. Hayward, 1999; Berkeley *et al.*, 2007), it is necessary to establish site-specific characteristics (Kosciuch *et al.*, 2018). Results from the modern sediment collection at Kujukuri provide a new modern dataset and will prove useful in constraining sediment provenance for tsunami deposits because taxonomic data clustered into two distinct biofacies (BF1 and BF2) representing offshore and onshore sources of sediment.

Along the Kujukuri shelf, foraminiferal assemblages varied with distance from the shoreline (Figs 2 and 3). For example, planktonic foraminifera are present in low abundances within the swash and foreshore environments (0 to 9% in T1; 4 to 12% in T2) and peak (17 to 48% in T1; 15 to 58% in T2) in the offshore zone at distances of >30 km from the shoreline. Planktonics are notably absent in all dune samples. The presence of planktonics has previously been used to document overwash deposits (Davies *et al.*, 2003; Hawkes *et al.*, 2007; Uchida *et al.*, 2010); however, the extent to which they accumulate in coastal sediments versus the extent to which they get washed in by a tsunami wave or storm surge is difficult to assess. Beach and dune sediments at Kujukuri do not contain high relative abundances of planktonic foraminifera, and therefore higher abundances within overwash deposits would indicate a contribution of offshore sediments from tens of kilometres seaward of the shoreline.

Similar to planktonics, *Ammonia parkinsoniana*, a foraminifer that is common in intertidal environments (Hayward *et al.*, 2004) was abundant in supratidal (12 to 23% in T1) and intertidal (15 to 30% in T1) samples, but much less so in offshore samples (0 to 4% in T1). This is consistent with the findings of Hayward & Hollis (1994) that report the occurrence of *Ammonia* in brackish intertidal and shallow subtidal sediments. Although abundances of robust-tested foraminifera such as *A. parkinsoniana* peaked in the intertidal zone where wave energy is the highest, species with thin-walled, fragile tests were more common in the offshore. For example, *Uvigerinella glabra* is generally absent from samples up to a distance of 6·6 km offshore (depth = −22 m above TP). This is consistent

with a study by Pilarczyk *et al.* (2011) where the fragile *Ammonia tepida* was limited to low-energy, protected areas within a lagoon, and the more robust-tested *Ammonia parkinsoniana* and *Ammonia convexa* were more abundant in the higher energy swash zone.

The taphonomic character of foraminifera varied predictably with distance from the shoreline. Calcareous foraminifera within the swash zone and deeper are sheltered from subaerial exposure and have the highest proportions of taphonomically unaltered individuals across all samples (for example, *ca* 45% unaltered in T2 swash sediments versus 0% in dune sediments). Increased residence time in the foreshore, backshore and dune environments causes foraminiferal tests to become increasingly corroded and abraded ('corraded'). For example, along T1, the average percentage of corraded individuals increased with increasing distance from the shoreline from 22% in the swash, to 41% in the foreshore, to 68% in the backshore, to 89% in the dune (Fig. 2). These findings are consistent with Pilarczyk *et al.* (2011) and Kosciuch *et al.* (2018) who report higher abundances of taphonomically unaltered foraminifera within subtidal environments relative to intertidal and subaerial sediments.

Fragmentation of foraminifera showed only a minor increase in abundance with increasing distance inland in both of the transects (Figs 2 and 3). Several studies report increased abundances of fragmented foraminifera within tsunami deposits (e.g. Kortekaas & Dawson, 2007; Chagué-Goff *et al.*, 2011). This suggests that fragmentation within tsunami deposits may be less reflective of the original depositional environment and more the result of overprinting by a tsunami.

Microfossil taphonomy, underutilized as a proxy in overwash studies (Mamo *et al.*, 2009; Pilarczyk *et al.*, 2014), showed the greatest relationship with increasing distance inland (Figs 2 and 3) and produced cluster scenarios with the highest average silhouette width. Tests that included taphonomic datasets were the only cases where separation between offshore, intertidal and supratidal zones could be made (*tests 2* and *4*; Fig. 5). This is similar to Kosciuch *et al.* (2018) who report that taphonomic datasets enhanced the utility of taxonomic datasets in a tropical reef flat environment. Studies by Goodman-Tchernov *et al.* (2016) and Hoffmann *et al.* (2018) used a subset of taphonomic characters of individual foraminifera in combination with archaeological and sedimentological evidence to document palaeotsunami deposits. Usami *et al.* (2017) used the presence of well-preserved tests from thin-walled (delicate) species to assess sediment transport by a turbidity current generated by the 2011 Tohoku tsunami. Collectively, these studies highlight the power of foraminiferal taphonomy; however, it is important to note that taphonomy should not be used as stand-alone technique. Rather, taphonomy is best used in combination with other proxies, such as taxonomy, where it can strengthen interpretations and provide ecological context.

Modern baseline studies and sediment provenance

Sediment provenance assessment is integral to the proper interpretation of overwash deposits and is particularly important when: (i) distinguishing overwash deposits from overlying or underlying sediments that are similar in composition (e.g. Pilarczyk *et al.*, 2011; Kelsey *et al.*, 2015; Kosciuch *et al.*, 2018); (ii) attempting to assess the magnitude of an event (Uchida *et al.*, 2010; Sieh *et al.*, 2015); and (iii) distinguishing between different types of events (for example, storm versus tsunami; Donato *et al.*, 2008; Switzer & Jones, 2008). Sedimentary and micropalaeontological proxies have previously been used to assess sediment provenance and interpret tsunami deposits (Hemphill-Haley, 1995; Hawkes *et al.*, 2007; Sawai *et al.*, 2009a,b; Chagué-Goff *et al.*, 2011); however, a quantitative means of determining which proxies are most effective in constraining sediment provenance is rarely used.

This study provides a new quantitative dataset of modern coastal and offshore sediments and foraminifera from Japan for the purpose of identifying and inferring the sediment provenance of tsunami deposits in the palaeorecord. The 2011 Tohoku tsunami impacted the Kujukuri shelf and coastline and may have resulted in persistent homogenization of the surface sediment. However, for the following reasons, this study assumed that the collected sediments indeed do represent normal background conditions: (i) the tsunami at this location resulted in <2 m of run up (Mori *et al.*, 2012); (ii) surface samples in this study were collected five years after the tsunami; (iii) sampling was restricted to the upper 1 cm of sediment; and (iv) clear zonations were evident, indicating a lack of homogenization by tsunami disturbance.

Studies of the rates of recovery of benthic faunal communities after major tsunami events have shown that in shallow marine environments, the complete recovery of the benthic community is possible after five days (Altaff *et al.*, 2005), within 50 days (Szczucinski *et al.*, 2006) or within several months (Yamada *et al.*, 2014). However, deeper continental slope benthic communities off south-east India had not fully recovered within 18 months of the 2004 Indian Ocean Tsunami (Khan *et al.*, 2018). Thus, the assumption that the Kujukuri shelf and coastline returned to pre-tsunami conditions is a likely one given the five-year difference between the tsunami and the collection of the surface samples analyzed in this study.

Using Partitioning Around Medoids (PAM) cluster analysis, two coastal zones (onshore and offshore) were objectively discriminated, and it was quantitatively determined which proxy datasets are most effective in constraining sediment provenance within these zones and which proxies will be most useful in documenting tsunami deposits at Kujukuri. The findings of this study show that, when compared with grain-size (average silhouette width = 0·40) and taxonomic (average silhouette width = 0·13) datasets, the surface condition of individual foraminifera (taphonomy; average silhouette width = 0·53 for a two-cluster scenario, 0·63 for a three-cluster scenario) was the best indicator of sediment provenance (Fig. 5; Table 1).

Foraminiferal taphonomy (*test 2*) was the only test where a three-cluster scenario produced the highest silhouette width (average silhouette width = 0·63) and made ecological sense, separating the sample sites into supratidal (86% of samples clustered appropriately), intertidal (93% of samples clustered appropriately) and offshore (100% of samples clustered appropriately) zones (Fig. 5). Although the highest average silhouette widths for *tests 1, 3* and *5* to *7* were produced under a three-cluster scenario, the clusters contained a mixture of samples from multiple zones and did not make ecological sense. For example, in a three-cluster scenario, taxonomic data assigned samples to the supratidal, intertidal and offshore zones with an accuracy of 50%, 40% and 100%, respectively. Accuracy was improved when the two-cluster scenario was used; 84% of samples were appropriately clustered in the onshore zone, while 94% of samples clustered appropriately in the offshore zone.

Kosciuch *et al.* (2018) used PAM cluster analysis to identify six zones in a modern carbonate reef environment from Vanuatu. Similar to the samples collected from Kujukuri, Kosciuch *et al.* (2018) found that taphonomic data produced clusters with a higher average silhouette width (0·46) than taxonomic data (0·28). However, unlike the present study, samples from the carbonate reef only clustered with 66% (taxonomy) and 64% (taphonomy) accuracy. The study from Vanuatu concluded that the combined use of taxonomy and taphonomy produced a cluster scenario with the highest percentage of appropriately clustered samples (94%). At Kujukuri, the combined use of taxonomy and taphonomy produced a three-cluster scenario where 73%, 85% and 100% of samples clustered appropriately (average accuracy = 88%) in the supratidal, intertidal and offshore zones, respectively (Fig. 5; *test 4*).

CONCLUSION

Detailed modern distributions of sedimentological proxies such as grain size, foraminiferal taxonomy and taphonomy will aid in the identification of tsunami deposits that are preserved in coastal sediments along eastern Japan because they identify sediment sources within coastal, nearshore and offshore environments. The identification of these sediment sources in the modern environment is important in assessing the provenance of tsunami deposits because they provide insight into how far and from what depth the sediments were transported by a tsunami wave.

Although a multi-proxy approach is necessary to properly assess tsunami deposits in the geological record, results from this study show that taphonomy, which is not commonly used in overwash studies, will be the most useful parameter for constraining sediment provenance and aiding in the interpretation of additional anomalous sand layers at this site, as well as other temperate locations. On the contrary, foraminiferal taxonomy, a common proxy used to assess overwash deposits, proved to be the least effective parameter in distinguishing offshore and onshore zones when used in isolation of other proxies. The results of this study show that the best combination of parameters for identifying the sediment source of tsunami deposits at Kujukuri will be taxonomy and taphonomy, while other studies document its use in discriminating tsunami deposits in the geological record. For these reasons, it is recommended that taphonomic analysis be applied

when assessing foraminiferal taxa in overwash deposits.

ACKNOWLEDGEMENTS

This work was supported by funding from the National Science Foundation (EAR 1624612) and the Japan Society for the Promotion of Science (15K05334). CG was supported by NUS start-up grant (R-109-000-223-133) and BPH was supported by the National Research Foundation Singapore and the Singapore Ministry of Education under the Research Centres of Excellence initiative. Offshore samples were obtained by AIST Research Project 'Investigations on Geology and Active Faults in the Coastal Zone of Japan'. Taku Ajioka is thanked for his assistance in shipboard sample collection. The manuscript benefitted from the thoughtful and productive comments of two anonymous reviewers. This work is a contribution to IGCP Project 639, 'Sea-level Change from Minutes to Millennia'. This is Earth Observatory of Singapore contribution number 233. The authors declare no conflicts of interest.

REFERENCES

Altaff, K., **Sugumaran, J.** and **Navee, S.** (2005) Impact of tsunami on meiofauna of Marina beach, Chennai, India. *Curr. Sci.*, **89**, 34–38.

Atwater, B.F. (1987) Evidence for great Holocene earthquakes along the outer coast of Washington State. *Science*, **236**, 942–944.

Berkeley, A., **Perry, C.T.**, **Smithers, S.G.**, **Horton, B.P.** and **Taylor, K.G.** (2007) A review of the ecological and taphonomic controls on foraminiferal assemblage development in intertidal environments. *Earth-Sci. Rev.*, **83**, 205–230.

Blott, S.J. and **Pye, K.** (2001) Gradistat: a grain size distribution and statistics package for the analysis of unconsolidated sediments. *Earth Surf. Process. Landf.*, **26**, 1237–1248.

Chagué-Goff, C., **Schneider, J.-L.**, **Goff, J.R.**, **Dominey-Howes, D.** and **Strotz, L.** (2011) Expanding the proxy toolkit to help identify past events – lessons from the 2004 Indian Ocean Tsunami and the 2009 South Pacific Tsunami. *Earth-Sci. Rev.*, **107**, 107–122.

Chagué-Goff, C., **Andrew, A.**, **Szczuciński, W.**, **Goff, J.** and **Nishimura, Y.** (2012) Geochemical signatures up to the maximum inundation of the 2011 Tohoku-oki tsunami – implication for the 869 AD Jogan and other paleotsunamis. *Sed. Geol.*, **282**, 65–77.

Cisternas, M., **Atwater, B.F.**, **Torrejon, F.**, **Sawai, Y.**, **Machuca, G.**, **Lagos, M.**, **Eipert, A.**, **Youlton, C.**, **Salgado, I.**, **Kamataki, T.**, **Shishikura, M.**, **Rajendran, C.P.**, **Malik, J.K.**, **Rizal, Y.** and **Husni, M.** (2005) Predecessors of the giant 1960 Chile earthquake. *Nature*, **437**, 404–407.

Davies, H.L., **Davies, J.M.**, **Perembo, R.C.B.** and **Lus, W.Y.** (2003) The Aitape 1998 tsunami: reconstructing the event from interviews and field mapping. *Pure Appl. Geophys.*, **160**, 1895–1922.

Davis, J.C. and **Sampson, R.J.** (2002) *Statistics and Data Analysis in Geology*, Vol. 3. Wiley, New York, 656 p.

Dawson, S., **Smith, D.E.**, **Ruffman, A.** and **Shi, S.** (1996) The diatom biostratigraphy of tsunami deposits: examples from recent and middle Holocene events. *Phys. Chem. Earth*, **21**, 87–92.

Donato, S.V., **Reinhardt, E.G.**, **Boyce, J.I.**, **Rothaus, R.** and **Vosmer, T.** (2008) Identifying tsunami deposits using bivalve shell taphonomy. *Geology*, **36**, 199–202.

Donato, S.V., **Reinhardt, E.G.**, **Boyce, J.I.**, **Pilarczyk, J.E.** and **Jupp, B.P.** (2009) Particle-size distribution of inferred tsunami deposits in Sur Lagoon, Sultanate of Oman. *Mar. Geol.*, **257**, 54–64.

Dura, T., **Hemphill-Haley, E.**, **Sawai, Y.** and **Horton, B.P.** (2016) The application of diatoms to reconstruct the history of subduction zone earthquakes and tsunamis. *Earth-Sci. Rev.*, **152**, 181–197.

Fujiwara, O. and **Kamataki, T.** (2007) Identification of tsunami deposits considering the tsunami waveform: an example of subaqueous tsunami deposits in Holocene shallow bay on southern Boso Peninsula, Central Japan. *Sed. Geol.*, **200**, 295–313.

Gao, S. and **Collins, M.B.** (1994) Analysis of grain size trends, for defining sediment transport pathways in marine environments. *J. Coast. Res.*, **10**, 70–78.

Gischler, E. and **Möder, A.** (2009) Modern benthic foraminifera on Banco Chinchorro, Quintana Roo, Mexico. *Facies*, **55**, 27–35.

Goff, J., **Lamarche, G.**, **Pelletier, B.**, **Chagué-Goff, C.** and **Strotz, L.** (2011) Predecessors to the 2009 South Pacific tsunami in the Wallis and Futuna archipelago. *Eart Sci. Rev.*, **107**, 91–106.

Goodman-Tchernov, B., **Katz, T.**, **Shaked, Y.**, **Qupty, N.**, **Kanari, M.**, **Niemi, T.** and **Agnon, A.** (2016) Offshore evidence for an undocumented tsunami event in the 'low risk' Gulf of Aqaba-Eilat, Northern Red Sea. *PLoS ONE*, **11**, e0145802.

Goto, K., **Chagué-Goff, C.**, **Goff, J.** and **Jaffe, B.** (2012) The future of tsunami research following the 2011 Tohoku-oki event. *Sed. Geol.*, **282**, 1–13.

Grand Pre, C.A., **Horton, B.P.**, **Kelsey, H.M.**, **Rubin, C.M.**, **Hawkes, A.D.**, **Daryono, M.R.**, **Rosenberg, G.** and **Culver, S.J.** (2012) Stratigraphic evidence for an early Holocene earthquake in Aceh, Indonesia. *Quatern. Sci. Rev.*, **54**, 142–151.

Hawkes, A.D. and **Horton, B.P.** (2012) Sedimentary record of storm deposits from Hurricane Ike, Galveston and San Luis Islands, Texas. *Geomorphology*, **171**, 180–189.

Hawkes, A.D., **Bird, M.**, **Cowie, S.**, **Grundy-Warr, C.**, **Horton, B.P.**, **Tan Shau Hwai, A.**, **Law, L.**, **Macgregor, C.**, **Nott, J.**, **Eong Ong, J.**, **Rigg, J.**, **Robinson, R.**, **Tan Mullins, M.**, **Tiong, T.**, **Yasin, Z.** and **Wan Aik, L.** (2007) Sediments deposited by the 2004 Indian Ocean tsunami along the Malaysia-Thailand Peninsula. *Mar. Geol.*, **242**, 169–190.

Hayward, B.W. (1999) *Recent New Zealand Shallow-Water Benthic Foraminifera: taxonomy, Ecologic Distribution, Biogeography, and Use in Paleoenvironmental Assessment*. Institute of Geological & Nuclear Sciences, Lower Hutt, NZ, 258 p.

Hayward, B.W. and **Hollis, C.J.** (1994) Brackish foraminifera in New Zealand: a taxonomic and ecological review. *Micropaleontology*, **40**, 185–222.

Hayward, B.W., **Holzmann, M.**, **Grenfell, H.R.**, **Pawlowski, J.** and **Triggs, C.M.** (2004) Morphological distinction of molecular types in Ammonia – towards a taxonomic revision of the world's most commonly misidentified foraminifera. *Mar. Micropaleontol.*, **50**, 237–271.

Hemphill-Haley, E. (1995) Diatom evidence for earthquake-induced subsidence and tsunami 300 years ago in southern coastal Washington. *Geol. Soc. Am. Bull.*, **107**, 367–378.

Hoffmann, N., **Master, D.** and **Goodman-Tchernov, B.** (2018) Possible tsunami inundation identified amongst 4–5th century BCE archaeological deposits at Tel Ashkelon. *Israel. Mar. Geol.*, **396**, 150–159.

Jaffe, B., **Buckley, M.**, **Richmond, B.**, **Strotz, L.**, **Etienne, S.**, **Clark, K.**, **Watt, S.**, **Gelfenbaum, G.** and **Goff, J.** (2011) Flow speed estimated by inverse modeling of sandy sediment deposited by the 29 September 2009 tsunami near Satitoa, east Upolu, Samoa. *Earth-Sci. Rev.*, **107**, 23–37.

Jiang, C., **Wu, Z.**, **Chen, J.**, **Deng, B.** and **Long, Y.** (2015) Sorting and sedimentology character of sand beach under wave action. *Procedia Eng.*, **116**, 771–777.

Kaufman, L. and **Rousseeuw, P.J.** (1990) Finding Groups in Data: An Introduction to Cluster Analysis. Wiley-Interscience, 342 pp.

Kelsey, H., **Engelhart, S.E.**, **Pilarczyk, J.E.**, **Horton, B.P.**, **Rubin, C.M.**, **Daryono, M.**, **Ismail, N.**, **Hawkes, A.D.**, **Bernhardt, C.** and **Cahill, N.** (2015) Accommodation space, relative sea level, and the archiving of paleo-earthquakes along subduction zones. *Geology*, **43**, 675–678.

Kemp, A.C., **Horton, B.P.**, **Vann, D.R.**, **Engelhart, S.E.**, **Grand Pre, C.A.**, **Vane, C.H.**, **Nikitina, D.** and **Anisfeld, S.C.** (2012) Quantitative vertical zonation of salt-marsh foraminifera for reconstructing former sea level; an example from New Jersey, USA. *Quatern. Sci. Rev.*, **54**, 26–39.

Khan, A.S., **Ravikuman, B.**, **Lyla, S.** and **Manokaran, S.** (2018) Impact of the 2004 tsunami on the macrofauna of the continental slope of the southeast coast of India. *Mar. Ecol.*, **39**(5), e12527.

Kortekaas, S. and **Dawson, A.G.** (2007) Distinguishing tsunami and storm deposits: an example from Martinhal, SW Portugal. *Sed. Geol.*, **200**, 208–221.

Kosciuch, T.J., **Pilarczyk, J.E.**, **Hong, I.**, **Fritz, H.M.**, **Horton, B.P.**, **Rarai, A.**, **Harrison, M.J.** and **Jockley, F.R.** (2018) Foraminifera reveal a shallow nearshore origin for overwash sediments deposited by Tropical Cyclone Pam in Vanuatu (South Pacific). *Mar. Geol.*, **396**, 171–185.

Krumbein, W.C. (1934) Size frequency distributions of sediments. *J. Sed. Petrol.*, **4**, 65–77.

Lane, P., **Donnelly, J.P.**, **Woodruff, J.D.** and **Hawkes, A.D.** (2011) A decadally-resolved paleohurricane record archived in the late Holocene sediments of a Florida sinkhole. *Mar. Geol.*, **287**, 14–30.

Loeblich, A.R. and **Tappan, H.** (1987) *Foraminiferal Genera and Their Classification*. Van Nostrand Reinhold Co., New York, NY, 2031 p.

Maechler, M., **Rousseeuw, P.**, **Struyf, A.** and **Hubert, M.** (2005) Cluster analysis basics and extensions R Statistics Package (CRAN).

Mamo, B., **Strotz, L.** and **Dominey-Howes, D.** (2009) Tsunami sediments and their foraminiferal assemblages. *Earth-Sci. Rev.*, **96**, 263–278.

Masuda, F., **Fujiwara, O.**, **Sakai, T.** and **Araya, T.** (2001) Relative sea-level changes and co-seismic uplifts over six millennia, preserved in beach deposits of the Kujukuri strand plain, Pacific coast of the Boso Peninsula, Japan (in Japanese with English abstract). *Chigaku Zasshi (J. Geogr.)*, **110**, 650–664.

Matsumoto, D., **Sawai, Y.**, **Tanigawa, K.**, **Fujiwara, O.**, **Namegaya, Y.**, **Shishikura, M.**, **Kagohara, K.** and **Kimura, H.** (2016) Tsunami deposit associated with the 2011 Tohoku-oki tsunami in the Hasunuma site of the Kujukuri coastal plain, Japan. *Isl. Arc*, **25**, 369–385.

Minoura, K. and **Nakaya, S.** (1991) Traces of tsunami preserved in inter-tidal lacustrine and marsh deposits: some examples from northeast Japan. *J. Geol.*, **99**, 265–287.

Mizuno, K. and **White, W.B.** (1983) Annual and interannual variability in the Kuroshio current system. *J. Phys. Oceanogr.*, **13**, 1847–1867.

Mori, N., **Takahashi, T.** and **The 2011 Tohoku Earthquake Tsunami Joint Survey Group** (2012) Nationwide post event survey and analysis of the 2011 Tohoku earthquake tsunami. *Coast. Eng. J.*, **54**, 1250001.

Moriwaki, H. (1979) The landform evolution of the Kujukuri coastal plain, central Japan (in Japanese with English abstract). *Daiyonki Kenkyu (Quatern. Res. Jpn.)*, **18**, 1–16.

Murray, J.W. and **Bowser, S.S.** (2000) Mortality, protoplasm decay rate, and reliability of staining techniques to recognize 'living' foraminifera: a review. *J. Foraminifer. Res.*, **30**, 66–70.

Namegaya, Y., **Satake, K.** and **Shishikura, M.** (2011) Fault models of the 1703 Genroku and 1923 Taisho Kanto earthquakes inferred from coastal movements in the southern Kanto area. *Ann. Rep. Active Fault Paleoearthquake Res.*, **11**, 107–120.

Nanayama, F. and **Shigeno, K.** (2006) Inflow and outflow facies from the 1993 tsunami in southwest Hokkaido. *Sed. Geol.*, **187**, 139–158.

Nanayama, F., **Satake, K.**, **Furukawa, R.**, **Shimokawa, K.**, **Atwater, B.F.**, **Shigeno, K.** and **Yamaki, S.** (2003) Unusually large earthquakes inferred from tsunami deposits along the Kuril trench. *Nature*, **424**, 660–663.

Nanayama, F., **Furukawa, R.**, **Shigeno, K.**, **Makino, A.**, **Soeda, Y.** and **Igarashi, Y.** (2007) Nine unusually large tsunami deposits from the past 4000 years at Kiritappu marsh along the southern Kuril Trench. *Sed. Geol.*, **200**, 275–294.

Nishida, N., **Ajioka, T.**, **Ikehara, K.**, **Nakashima, R.** and **Utsunomiya, M.** (2019) Spatial variation and stratigraphy of the marine sediments off the east of the Boso Peninsula, Pacific Ocean, Japan. In: *Seamless Geoinformation of Coastal Zone, "Eastern Coastal Zone of Boso Peninsula"* (Ed. K. Arai) Seamless Geological Map of Coastal Zone S-6, Geological Survey of Japan, AIST (in Japanese with English abstract). Available at: https://www.gsj.jp/researchs/project/coastal-geology/results/s-6.html

Pham, D.T., **Gouramanis, C.**, **Switzer, A.D.**, **Rubin, C.M.**, **Jones, B.G.**, **Jankaew, K.** and **Carr, P.F.** (2017) Elemental and mineralogical analysis of marine and coastal sediments from Phra Thong Island, Thailand: insights into the provenance of coastal hazard deposits. *Mar. Geol.*, **385**, 274–292.

Pilarczyk, J.E., **Reinhardt, E.G.**, **Boyce, J.I.**, **Schwarcz, H.P.** and **Donato, S.V.** (2011) Assessing surficial foraminiferal distributions as an overwash indicator in Sur Lagoon, Sultanate of Oman. *Mar. Micropaleontol.*, **80**, 62–73.

Pilarczyk, J.E., **Horton, B.P.**, **Witter, R.C.**, **Vane, C.H.**, **Chagué-Goff, C.** and **Goff, J.** (2012) Sedimentary and foraminiferal evidence of the 2011 Tohoku-oki tsunami on the Sendai coastal plain, Japan. *Sed. Geol.*, **282**, 78–89.

Pilarczyk, J.E., **Dura, T.**, **Horton, B.P.**, **Engelhart, S.E.**, **Kemp, A.C.** and **Sawai, Y.** (2014) Microfossils from coastal environment as

indicators of paleo-earthquakes, tsunamis and storms. *Palaeogeogr. Palaeoclimatol. Palaeoecol.*, **413**, 144–157.

Pinegina, T.K., **Bourgeois, J.**, **Bazanova, L.I.**, **Melekestsev, I.V.** and **Braitseva, O.A.** (2003) A millennial-scale record of Holocene tsunamis on the Kronotskiy Bay coast, Kamchatka, Russia. *Quatern. Res.*, **59**, 36–47.

Sambridge, M., **Braun, J.** and **McQueen, H.** (1995) Geophysical parametrization and interpolation of irregular data using natural neighbors. *Geophys. J. Int.*, **122**, 837–857.

Sawai, Y., **Satake, K.**, **Kamataki, T.**, **Nasu, H.**, **Shishikura, M.**, **Atwater, B.F.**, **Horton, B.P.**, **Kelsey, H.M.**, **Nagumo, T.** and **Yamaguchi, M.** (2004) Transient uplift after a 17th-century earthquake along the Kuril subduction zone. *Science*, **306**, 1918–1920.

Sawai, Y., **Jankaew, K.**, **Martin, M.E.**, **Prendergast, A.**, **Choowong, M.** and **Charoentitirat, T.** (2009a) Diatom assemblages in tsunami deposits associated with the 2004 Indian Ocean tsunami at Phra Thong Island, Thailand. *Mar. Micropaleontol.*, **73**, 70–79.

Sawai, Y., **Kamataki, T.**, **Shishikura, M.**, **Nasu, H.**, **Okamura, Y.**, **Satake, K.**, **Thomson, K.H.**, **Matsumoto, D.**, **Fujii, Y.**, **Komatsubara, J.** and **Aung, T.T.** (2009b) Aperiodic recurrence of geologically recorded tsunamis during the past 5500 years in eastern Hokkaido, Japan. *J. Geophys. Res. Solid Earth*, **114**, B01319. https://doi.org/10.1029/2007JB005503.

Sawai, Y., **Namegaya, Y.**, **Okamura, Y.**, **Satake, K.** and **Shishikura, M.** (2012) Challenges of anticipating the 2011 Tohoku earthquake and tsunami using coastal geology. *Geophys. Res. Lett.*, **39**, L21309. https://doi.org/10.1029/2012GL053692.

Sawai, Y., **Namegaya, Y.**, **Tamura, T.**, **Nakashima, R.** and **Tanigawa, K.** (2015) Shorter intervals between great earthquakes near Sendai: scour ponds and a sand layer attributable to A.D. 1454 overwash. *Geophys. Res. Lett.*, **42**, 4795–4800.

Scott, D.B. and **Hermelin, J.O.R.** (1993) A device for precision splitting of micropaleontological samples in liquid suspension. *J. Paleontol.*, **67**, 151–154.

Shinozaki, T., **Fujino, S.**, **Ikehara, M.**, **Sawai, Y.**, **Tamura, T.**, **Goto, K.**, **Sugawara, D.** and **Abe, T.** (2015) Marine biomarkers deposited on coastal land by the 2011 Tohoku-oki tsunami. *Nat. Hazards*, **77**, 445–460.

Shishikura, M. (2000) Coseismic vertical displacement in the Boso Peninsula during the 1703 Genroku Kanto earthquake, deduced from emerged shoreline topography. *Rekishi Jishin*, **16**, 113–122. (in Japanese with English abstract).

Shishikura, M. (2001) Crustal movements in the Boso Peninsula from the analysis of height distribution of the highest Holocene paleo-shoreline. Annual Report on Active Fault and Paleoearthquake Researches 1. Active Fault Research Center, AIST, pp. 273–285 (in Japanese with English abstract).

Shishikura, M. (2014) History of the paleo-earthquakes along the Sagami Trough, central Japan: review of coastal paleo-seismological studies in the Kanto region. *Episodes*, **37**, 246–257.

Shishikura, M. and **Miyauchi, T.** (2001) Holocene geomorphic development related to seismotectonics in coastal lowlands of the Boso Peninsula, Central Japan. *Quatern. Res. (Japan)*, **40**, 235–242. (in Japanese).

Sieh, K., **Daly, P.**, **McKinnon, E.E.**, **Pilarczyk, J.E.**, **Chiang, H.W.**, **Horton, B.**, **Rubin, C.M.**, **Shen, C.C.**, **Ismail, N.**, **Vane, C.H.** and **Feener, R.M.** (2015) Penultimate predecessors of the 2004 Indian Ocean tsunami in Aceh, Sumatra: stratigraphic, archaeological, and historical evidence. *J. Geophys. Res. Solid Earth*, **120**, 308–325.

Sunamura, T. and **Horikawa, K.** (1977) Sediment budget in Kujukuri coastal area, Japan. Coastal Sediments '77. American Society of Civil Engineers, 475-487.

Switzer, A.D. and **Jones, B.G.** (2008) Large-scale washover sedimentation in a freshwater lagoon from the southeast Australian coast: sea-level change, tsunami, or exceptionally large storm? *Holocene*, **18**, 787–803.

Szczucinski, W., **Chaimanee, N.**, **Niedzielski, P.**, **Rachlewicz, G.**, **Saisuttichai, D.**, **Tepsuwan, T.**, **Lorenc, S.** and **Siepak, J.** (2006) Environmental and geological impacts of the 26 December 2004 tsunami in coastal zone of Thailand – overview of short and long-term effects. *Pol. J. Environ. Stud.*, **15**, 793–810.

Tamura, T., **Nanayama, F.**, **Saito, Y.**, **Murakami, F.**, **Nakashima, R.** and **Watanabe, K.** (2007) Intra-shoreface erosion in response to rapid sea-level fall: depositional record of a tectonically uplifted strand plain, Pacific coast of Japan. *Sedimentology*, **54**, 1149–1162.

Tamura, T., **Murakami, F.**, **Nanayama, F.**, **Watanabe, K.** and **Saito, Y.** (2008) Ground-penetrating radar profiles of Holocene raised-beach deposits in the Kujukuri stand plain, Pacific coast of eastern Japan. *Mar. Geol.*, **248**, 11–27.

Tamura, T., **Murakami, F.** and **Watanabe, K.** (2010) Holocene beach deposits for assessing coastal uplift of the northeastern Boso Peninsula, Pacific coast of Japan. *Quatern. Res.*, **74**, 227–234.

Tanigawa, K., **Sawai, Y.**, **Shishikura, M.**, **Namegaya, Y.** and **Matsumoto, D.** (2014) Geological evidence for an unusually large tsunami on the Pacific coast of Aomori, northern Japan. *J. Quatern. Sci.*, **29**, 200–208.

Uchida, J., **Fujiwara, O.**, **Hasegawa, S.** and **Kamataki, T.** (2010) Sources and depositional processes of tsunami deposits: analysis using foraminiferal tests and hydrodynamic verification. *Isl. Arc*, **19**, 427–442.

Uda, T. (1989) Comparative study on long-term shoreline evolution during the past 6000 years and recent short-term beach changes on the Kujukuri coast. *Chikei (Trans. Jpn. Geomorph. Uni.)*, **10**, 343–355 (in Japanese with English abstract).

Usami, K., **Ikehara, K.**, **Jenkins, R.G.** and **Ashi, J.** (2017) Benthic foraminiferal evidence of deep-sea sediment transport by the 2011 Tohoku-oki earthquake and tsunami. *Mar. Geol.*, **384**, 214–224.

Walton, W.R. (1952) Techniques for recognition of living foraminifera. *Cushman Found. Foram. Res.*, **3**, 56–60.

Yamada, K., **Terakura, M.** and **Tsukawaki, S.** (2014) The impact on bottom sediments and ostracods in the Khlong Thom River mouth following the 2004 Indian Ocean Tsunami. *Paleontol. Res.*, **18**, 104–117.

Manuscript received 1 May 2018; revision accepted 15 February 2019

Supporting Information

Additional information may be found online in the Supporting Information section at the end of the article:

Figure S1. Results of PAM cluster analysis for T1 showing tests 1 to 3 (a) to (c). (i) Average silhouette

width for 2, 3, 4 and 5 clusters. Highest average silhouette width (indicating the strongest structure) for each test is indicated by a dashed line. Silhouette plots of taxonomic (test 1), taphonomic (test 2) and grain-size (test 3) datasets divided into 2 (ii), 3 (iii), 4 (iv) and 5 (v) clusters. Grey and white bars differentiate between clusters. The average silhouette width is indicated by a dashed line.

Figure S2. Results of PAM cluster analysis for T1 showing tests 4 to 6 (d) to (f). (i) Average silhouette width for 2, 3, 4 and 5 clusters. Highest average silhouette width (indicating the strongest structure) for each test is indicated by a dashed line. Silhouette plots of taxonomic + taphonomic (test 4), taxonomic + taphonomic + grain size (test 5), taxonomic + grain-size (test 6) datasets divided into 2 (ii), 3 (iii), 4 (iv) and 5 (v) clusters. Grey and white bars differentiate between clusters. The average silhouette width is indicated by a dashed line.

Figure S3. Results of PAM cluster analysis for T1 showing test 7 (g). (i) Average silhouette width for 2, 3, 4 and 5 clusters. Highest average silhouette width (indicating the strongest structure) for each test is indicated by a dashed line. Silhouette plots of taphonomic + grain-size (test 7) datasets divided into 2 (ii), 3 (iii), 4 (iv) and 5 (v) clusters. Grey and white bars differentiate between clusters. The average silhouette width is indicated by a dashed line.

Figure S4. Results of PAM cluster analysis for T2 showing tests 1 to 3 (a) to (c). (i) Average silhouette width for 2, 3, 4 and 5 clusters. Highest average silhouette width (indicating the strongest structure) for each test is indicated by a dashed line. Silhouette plots of taxonomic (test 1), taphonomic (test 2) and grain-size (test 3) datasets divided into 2 (ii), 3 (iii), 4 (iv) and 5 (v) clusters. Grey and white bars differentiate between clusters. The average silhouette width is indicated by a dashed line.

Figure S5. Results of PAM cluster analysis for T2 showing tests 4 to 6 (d) to (f). (i) Average silhouette width for 2, 3, 4 and 5 clusters. Highest average silhouette width (indicating the strongest structure) for each test is indicated by a dashed line. Silhouette plots of taxonomic + taphonomic (test 4), taxonomic + taphonomic + grain-size (test 5), taxonomic + grain-size (test 6) datasets divided into 2 (ii), 3 (iii), 4 (iv) and 5 (v) clusters. Grey and white bars differentiate between clusters. The average silhouette width is indicated by a dashed line.

Figure S6. Results of PAM cluster analysis for T2 showing test 7 (g). (i) Average silhouette width for 2, 3, 4 and 5 clusters. Highest average silhouette width (indicating the strongest structure) for each test is indicated by a dashed line. Silhouette plots of taphonomic + grain-size (test 7) datasets divided into 2 (ii), 3 (iii), 4 (iv) and 5 (v) clusters. Grey and white bars differentiate between clusters. The average silhouette width is indicated by a dashed line.

Figure S7. Results of PAM cluster analysis for T1 + T2 showing tests 1 to 2 (a) to (b). (i) Average silhouette width for 2, 3, 4 and 5 clusters. Highest average silhouette width (indicating the strongest structure) for each test is indicated by a dashed line. Silhouette plots of taxonomic (test 1), and taphonomic (test 2) datasets divided into 2 (ii), 3 (iii), 4 (iv) and 5 (v) clusters. Grey and white bars differentiate between clusters. The average silhouette width is indicated by a dashed line.

Figure S8. Results of PAM cluster analysis for T1 + T2 showing tests 3 to 4 (c) to (d). (i) Average silhouette width for 2, 3, 4 and 5 clusters. Highest average silhouette width (indicating the strongest structure) for each test is indicated by a dashed line. Silhouette plots of grain-size (test 3) and taxonomic + taphonomic (test 4) datasets divided into 2 (ii), 3 (iii), 4 (iv) and 5 (v) clusters. Grey and white bars differentiate between clusters. The average silhouette width is indicated by a dashed line.

Figure S9. Results of PAM cluster analysis for T1 + T2 showing tests 5 to 6 (e) to (f). (i) Average silhouette width for 2, 3, 4 and 5 clusters. Highest average silhouette width (indicating the strongest structure) for each test is indicated by a dashed line. Silhouette plots of taxonomic + taphonomic + grain-size (test 5) and taxonomic + grain-size (test 6) datasets divided into 2 (ii), 3 (iii), 4 (iv) and 5 (v) clusters. Grey and white bars differentiate between clusters. The average silhouette width is indicated by a dashed line.

Figure S10. Results of PAM cluster analysis for T1 + T2 showing test 7 (g). (i) Average silhouette width for 2, 3, 4 and 5 clusters. Highest average silhouette width (indicating the strongest structure) for each test is indicated by a dashed line. Silhouette plots of taphonomic + grain-size (test 7) datasets divided into 2 (ii), 3 (iii), 4 (iv) and 5 (v) clusters. Grey and white bars differentiate between clusters. The average silhouette width is indicated by a dashed line.

Table S1. Grain-size statistics for T1.

Table S2. Grain-size statistics for T2.

Table S3. Foraminiferal taxonomic and taphonomic abundance data for T1 samples. Beach zone, distance from shoreline (m) and elevation (m above TP) are indicated.

Table S4. Foraminiferal taxonomic and taphonomic abundance data for T2 samples. Beach zone, distance from shoreline (m) and elevation (m above TP) are indicated.